Optical extinction spectrum of a single metal nanoparticle: Quantitative characterization of a particle and of its local environment

O. L. Muskens, P. Billaud, M. Broyer, N. Del Fatti,* and F. Vallée
LASIM, Université Lyon 1 and CNRS, 43 Bd. du 11 Novembre, 69622 Villeurbanne, France
(Received 19 June 2008; revised manuscript received 13 October 2008; published 10 November 2008)

Optical absorption spectroscopy of a single metal nanoparticle is used to characterize its properties and to obtain quantitative information on its local environment. Experiments were performed using the spatial modulation spectroscopy (SMS) technique on 16 nm mean diameter gold nanoparticles embedded in different medium (i.e., deposited on glass or embedded in a polymer layer). Extraction of the nanoparticle characteristics and determination of the dielectric constant of its environment are discussed, focusing on the impact of the particle shape assumption. The refractive index of the local environment deduced from these measurements shows large particle-to-particle variation, yielding information about fluctuations of the dielectric properties of the surrounding medium on a nanometric scale, inaccessible in ensemble measurements. The influence of the environment of a nanoparticle on its optically extracted geometry and its surface plasmon resonance broadening by surface effect are also studied at a single-particle level.

DOI: 10.1103/PhysRevB.78.205410 PACS number(s): 78.67.Bf, 78.40.Kc

I. INTRODUCTION

Size reduction effects and the concomitant increase of the role of the surfaces or interfaces are key parameters in the optical properties of nano-objects. In the case of metal, their main consequence is the appearance of resonances, the local surface plasmon resonances (SPR), in their linear and nonlinear optical responses.[1–3] These reflect local enhancement of the electromagnetic field in and around the metal nanoparticle due to the resonant response of the electrons of the metal. The spectral characteristics of the SPR, peak wavelength, resonance shape, and light absorption and scattering cross sections, are very sensitive to the properties of the nanoparticles (composition, structure, shape, and size) and of their surrounding (matrix, bound molecules or other particles).[1,3–9] To a certain extent, they can thus be adjusted to a given requirement, provided the nano-object geometry and environment are well controlled. It opens up many possibilities for manipulation of the optical field at a nanoscale and for adapting or enhancing the linear or nonlinear optical response of a nanoparticle or of a nearby object.[1–3,10–13] These sensitivities are also making the optical response of metal nanoparticles a large potential tool for nanoscale characterization of the particles themselves, provided their optical response is precisely modeled,[14] and of their local environment exploiting them as nanosensors.[15]

However, when ensembles of nanoparticles are optically investigated, the observed effects and the obtained information are averaged over the distribution of particle geometry and environment. This limitation can be circumvented studying a single particle. For a very weakly luminescent object such as a metallic nanoparticle it requires monitoring its direct interaction with light, i.e., its scattering or absorption of an incident light beam. Near-field optical technique [scanning near-field optical microscopy (SNOM)] has first been used to detect single metal nanoparticles.[16,17] The intrinsic difficulty of the interpretation of these measurements, due to perturbation of the particle environment by the tip,[18] has fostered the development of far-field techniques. The optical investigations of a single metal nanoparticle were performed using dark-field microscopy allowing for background-free detection of nanoparticle scattering.[19–22] As scattering efficiency scales as the square of the particle volume,[1,3,4] these methods are limited to large size particles, typically more than 20 nm. This fosters the development of novel approaches based either on heterodyne detection of light-scattering[23] or on direct[14,24] or indirect (via the induced environment heating)[25] detection of light absorption that dominates the small particle optical response.

The large reduction in the detection limit permitted by the latter absorption-based methods is particularly interesting for using single nanoparticles as nanosensors.[15,26,27] Actually, the SPR wavelength of a particle being sensitive to its dielectric surrounding over a region on the order of its size,[28] the SPR wavelength contains information on its environment over a volume that is concomitantly reduced with the particle size. In particular, in the context of plasmonic nanosensors based on molecular detection via the induced SPR wavelength shift, this offers a large potential for single-molecule sensing.[15,29] Depending on the geometry of the nanoparticle, its local environment and its modifications translate differently in its SPR properties.[1,27] Development of high-sensitivity single-nanoparticle nanosensors and extraction of quantitative information thus requires precise characterization of the used nanoparticle. It has been recently shown that such characterization can be done optically by quantitatively measuring the extinction cross-section spectrum of the nanoparticle using the spatial modulation spectroscopy (SMS) technique.[14,24,30,31] We have used this approach to investigate model systems formed by single quasispherical gold nanoparticles deposited on a substrate in air or embedded in a polymer (PVOH). After introducing the SMS technique, optical characterization of a nanoparticle and determination of the dielectric constant of its local environment are discussed focusing in particular on the impact of the assumed particle shape on the extracted information. Statistic of the analysis performed on different nanoparticles shows that the absolute value of the extinction of a single nanoparticle is modified by

its environment beyond that predicted by the change in its refractive index, suggesting enhanced absorption or modification of the surface of a particle by its environment.

II. EXPERIMENTAL METHOD

The SMS technique is based on modulating the position of a nanoparticle in the focal spot of a tightly focused light beam. For a particle much smaller than the beam size whose position is modulated along the y direction around its mean position (x,y) in the focal plane, the total beam extinction at the wavelength λ is given by[24]

$$\Delta P(x,y,\lambda) = -\sigma_{\text{ext}}(\lambda) I_\lambda[x, y + \delta_y \sin(2\pi f t)], \qquad (1)$$

where σ_{ext} is the particle extinction cross section and $I(x,y)$ is the beam intensity profile. f and δ_y are the modulation frequency and amplitude, respectively. If the latter is much smaller than the beam size, one can readily show that the modulated part of the transmitted power at the fundamental frequency f and its harmonic $2f$ are proportional to σ_{ext}:

$$\Delta P_f(x,y,\lambda) \approx -\sigma_{\text{ext}} \delta_y \frac{\partial I_\lambda(x,y)}{\partial y} \sin(2\pi f t),$$

$$\Delta P_{2f}(x,y,\lambda) \approx \frac{1}{4}\sigma_{\text{ext}}(\lambda)\delta_y^2 \frac{\partial^2 I_\lambda(x,y)}{\partial y^2} \cos(4\pi f t). \qquad (2)$$

When scanning the nanoparticle position in the focal plane, the modulated part of the transmitted power at f or $2f$ shows a profile proportional to the first or second derivative of the beam intensity $I(x,y)$ along the y direction, respectively. A profile directly proportional to $I(x,y)$ is obtained along the x direction. In both cases, the amplitude of the modulated signal is proportional to the absolute cross section $\sigma_{\text{ext}}(\lambda)$ of the investigated particle. Provided the modulation amplitude and the beam profile are known, it can thus be directly measured.[24]

For the modulation amplitudes comparable to the beam size used in the experiments, $\Delta P_{f,2f}$ has to be calculated numerically using Eq. (1). Derivative-like x-y profile is obtained similar to the very small amplitude regime [Eq. (2)] with, however, significant distortion when δ_y approaches the beam size. This is illustrated in Fig. 1, assuming Gaussian intensity profile $I(x,y)$ with a full width at half maximum d_{FWHM}. A maximum change in the sample transmission due to the presence of the nanoparticle $\Delta T_{f,2f}/T = \Delta P_{f,2f}/P$ is obtained for a vibrational amplitude $\delta_y^{\text{opt}} \approx 0.8 d_{\text{FWHM}}$ and $\approx d_{\text{FWHM}}$ for detection at f and $2f$, respectively (Fig. 2). Importantly, the sensitivity of the amplitude of $|\Delta T_{f,2f}/T|_{\max}$ on δ_y is largely reduced around δ_y^{opt}, making determination of σ_{ext} only weakly sensitive on this parameter.

The spatial resolution of the measurements is determined by the focal spot size d_{FWHM} and the modulation amplitude δ_y. As a first approximation, we defined it as the distance between the extrema of $|\Delta T_f/T|$ or the two side peaks of $|\Delta T_{2f}/T|$ (Fig. 1). It remains almost constant, close to d_{FWHM} for small modulation amplitude, and increases as δ_y approaches the beam size. For the optimal amplitudes, δ_y^{opt}, spatial resolution is only slightly degraded and these values

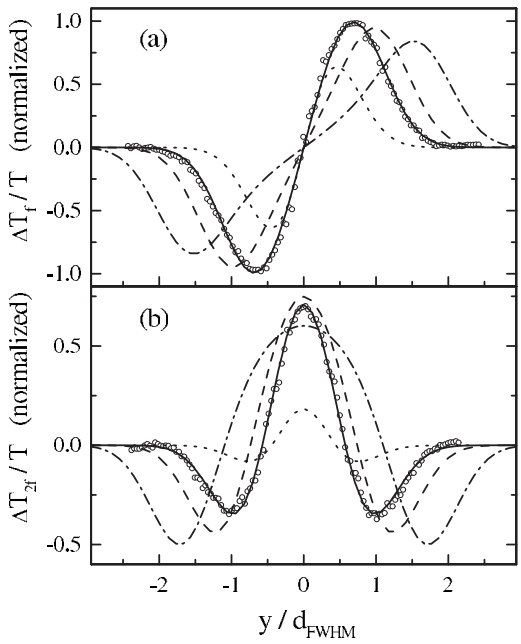

FIG. 1. Computed y-direction profile of the relative transmission change $\Delta T_{f,2f}/T$ modulated at (a) f or (b) $2f$ in a spatial modulation experiment. A Gaussian laser beam focused at $(x=0, y=0)$ on an absorbing nano-object at (x,y) much smaller than the focal spot diameter d_{FWHM} has been assumed. The dotted, full, dashed, and dash-dotted lines correspond to different normalized modulation amplitude in the y direction $\delta_y/d_{\text{FWHM}}=0.3, 0.82, 1.2$ and 1.7, respectively. The open dots are the results of measurements on a 15 nm gold nanoparticle performed at a laser wavelength of 532 nm with $d_{\text{FWHM}}=0.34$ μm and $\delta_y=0.28$ μm.

are systematically used in our SMS measurements. Note that observation of the full x-y spatial profile of $|\Delta T_{f,2f}/T|$ permits a spatial localization of the nanoparticle under study with a much better precision than the estimated spatial resolution.

The experimental setup for tunable wavelength measurements is shown in Fig. 3. The light beam is focused to a spot of several hundred nanometers in diameter onto the sample surface by a 100× microscope objective (N.A.=0.8). The sample is formed by isolated nanoparticles (i.e., separated by more than the beam size) dispersed on a glass substrate. Its position is modulated at $f \approx 1.5$ kHz by means of a piezoelectric element and mounted on a X-Y piezoelectric translation stage to record surface images. The transmitted light power is detected by a photodiode and demodulated at f or $2f$ using a lock-in amplifier. The setup achieves a sensitivity in $\Delta T/T$ of about 10^{-5} using a laser source with a few μW power, allowing the detection of the absorption cross section of gold nanoparticles as small as 5 nm,[24] i.e., a sensitivity in terms of extinction cross section down to about 5 nm^2.

The medium-brightness (typically a few μW in the selected bandwidth of 3 nm) and broadly tunable source in the visible range required for spectroscopic measurements is obtained by generation of a supercontinuum in a photonic crystal fiber.[32] In our setup, this is created by injecting the fiber with the 20 fs pulse train of a homemade Ti:sapphire femtosecond oscillator. The supercontinuum is subsequently dis-

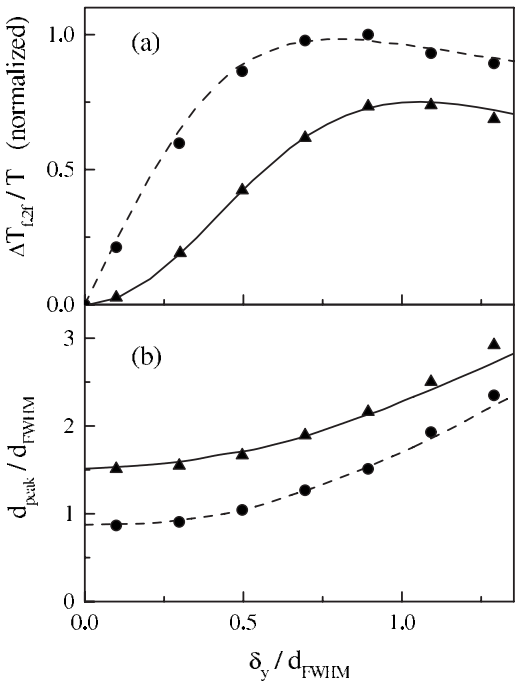

FIG. 2. (a) Dependence on the normalized modulation amplitude $\delta_y/d_{\mathrm{FWHM}}$ of the computed and measured amplitudes of the relative transmission change $\Delta T_{f,2f}/T$ modulated at f (dashed line and dots, respectively) and $2f$ (full line and triangles, respectively). (b) Calculated and measured dependence on the modulation amplitude of the spatial resolution of a spatial modulation experiment defined as the distance $d_{\mathrm{peak}}/d_{\mathrm{FWHM}}$ between the extrema of $|\Delta T_f/T|$ or the two side peaks of $|\Delta T_{2f}/T|$ for f (dashed line and dots) or $2f$ (full line and triangles) detection, respectively. Measurements were performed on a 15 nm gold nanoparticle at a laser wavelength of 532 nm with $d_{\mathrm{FWHM}}=0.34$ μm and $\delta_y=0.28$ μm.

persed by a grating pair separated by a −1 magnification telescope and frequency filtered using a slit (Fig. 3).[33] The created tunable source is unpolarized allowing measurement of both the unpolarized as well as polarized spectra (after insertion of a polarizer).

In the present investigation, samples with low surface density of nanoparticles were prepared by spin coating onto a glass substrate a colloidal solution of citrate-stabilized quasispherical gold particles (Sigma-Aldrich) with mean diameter 16.2 nm. Different samples were prepared with or without addition of a polymer (PVOH) in the solution. To exclude effects of the deposition history, polymer embedded particles were also prepared by adding a droplet of polymer after spin coating the particles. Nanoparticles deposited on glass or embedded in a thin polymer layer were thus obtained with a surface density of less than one particle per μm^2.

The y profile of the transmission change measured at f or $2f$ for a single gold nanoparticle with a laser source at 532 nm is in excellent agreement with the computed one (Fig. 1). Similar results are obtained using the supercontinuum source as illustrated by the x-y profile of the absolute value of the transmission change $|\Delta T_{2f}/T|$ measured at $\lambda=520$ nm (Fig. 4). As expected, it consists of three symmetric peaks along

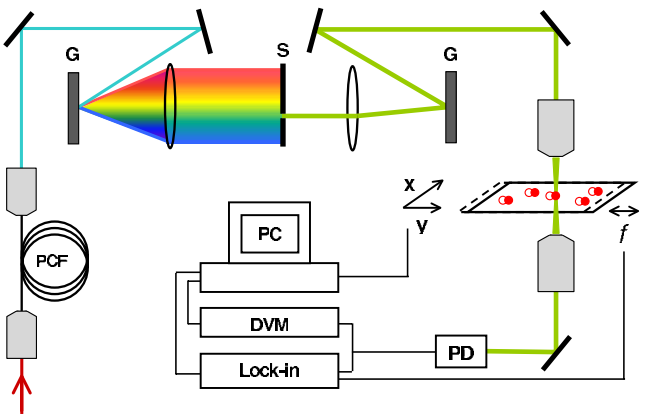

FIG. 3. (Color online) Experimental setup, showing the transmission microscope with piezoelectric sample translation at frequency f and x-y scanner, the signal detection and acquisition system consisting of a silicon photodiode, lock-in amplifier, digital voltmeter (DVM) and personal computer, and the tunable light source using a photonic crystal fiber (PCF), a grating pair (G) and a slit (S).

the modulation direction y and of a Gaussian shape along the perpendicular one x. The latter directly reflects the focal spot shape and size along x and permits their precise measurement [Eq. (2)]. Sections along the x direction show that the intensity profile is very well reproduced by a Gaussian shape with $d_{\mathrm{FWHM}}=0.35$ μm at $\lambda=520$ nm (Fig. 4, top). No anisotropy in the focal spot size and shape has been observed indicating that astigmatism is negligible in our setup. Similar analysis of single-particle images taken at different wavelengths yield precise experimental calibration of the disper-

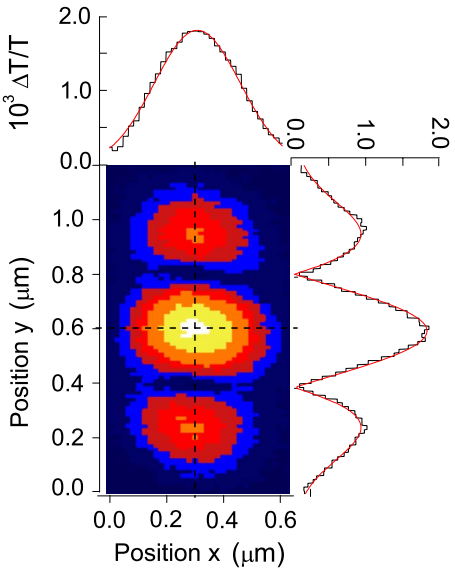

FIG. 4. (Color online) Image at $\lambda=520$ nm of a single gold particle and its x (top) and y (right) sections at the position of the dotted lines. The full lines are fits to a Gaussian beam profile with $d_{\mathrm{FWHM}}=0.35$ μm (x direction) and the numerically calculated $2f$ response (y direction) for the same d_{FWHM} and an oscillation amplitude $\delta_y=0.28$ μm. The absolute value of the signal amplitude is set by the extinction cross section yielding $\sigma_{\mathrm{ext}}=455\pm20$ nm^2.

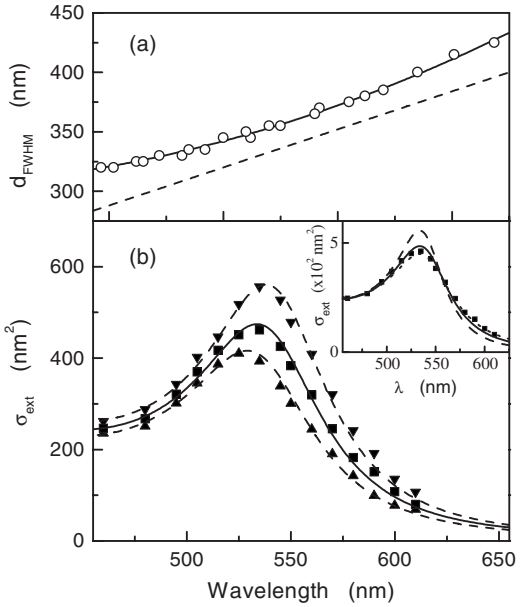

FIG. 5. (a) Dispersion of the diameter of the focal spot d_{FWHM} deduced from *X*-*Y* scans on a single gold nanoparticle. The full line is a polynomial fit of the experimental data. The dashed line shows the diffraction limit, $d_{\mathrm{FWHM}}=0.64\lambda$. (b) Extinction cross-section spectrum of a $D=20.3$ nm gold nanoparticle in PVOH, for unpolarized light (squares) and linearly polarized along the experimentally determined main particle axes (up- and down-triangles). The full and dashed lines are fits assuming a spherical and elliptical oblate particle, respectively. The inset shows the unpolarized data together with a fit using $g=0$, 0.8, and 1.3 (dashed, full, and dotted lines, respectively).

sion of d_{FWHM}. It has been reproduced phenomenologically using a second-order polynomial function in λ [Fig. 5(a)].

The shape of the *y* profile of the transmission change measured in real space is set by the beam size and modulation amplitude, also permitting further control of the value of these parameters. The full amplitude of $\Delta T_{f,2f}/T$ is directly set by the nanoparticle extinction cross section, $\sigma_{\mathrm{ext}}(\lambda)$. Numerically reproducing $\Delta T_f/T$ or $\Delta T_{2f}/T$ using Eq. (1), its absolute value and its spectrum can thus be obtained by measuring the *x*-*y* nanoparticle response for different wavelengths followed by precise analysis of its shape and amplitude.[24] However, after precise calibration of the setup, such full analysis is not necessary and $\sigma_{\mathrm{ext}}(\lambda)$ can be directly deduced from the $|\Delta T_{f,2f}/T|$ maximum amplitude. The precision of this approach has been confirmed by the excellent agreement between the σ_{ext} value measured by SMS and the computed ones from the nanoparticle geometry determined by transmission electron microscopy (TEM).[30]

III. SINGLE-PARTICLE SPECTRA

A. Unpolarized spectra

The extinction spectrum of a single gold nanoparticle measured with unpolarized light is shown in Fig. 5(b). Measurements are limited to wavelengths smaller than about 620 nm because of the limited power of the supercontinuum source for longer wavelengths, around the zero dispersion of the photonic crystal fiber (at 650 nm). As information on its anisotropy is lost (see below), the data were fitted assuming a spherical nanoparticle of diameter *D* embedded in a transparent medium with dielectric constant ϵ_m. For the small particles investigated here, $\sigma_{\mathrm{ext}}\approx\sigma_{\mathrm{abs}}$ (the scattering cross section is about 100 times smaller than the absorption one for a 20 nm gold nanoparticle at its SPR) and σ_{abs} can be approximated by its dipolar expression,[1,4]

$$\sigma_{\mathrm{abs}}(\lambda)=\frac{18\pi V\epsilon_m^{3/2}}{\lambda}\frac{\epsilon_2(\lambda)}{|\epsilon(\lambda)+2\epsilon_m|^2}, \tag{3}$$

where *V* is the particle volume and $\epsilon=\epsilon_1+i\epsilon_2$ is the metal dielectric constant. This expression yields an excellent approximation of the full Mie theory for the gold nanoparticles investigated here with sizes in the 20 nm range, and, in particular, of their SPR wavelengths.[34] If ϵ_2 is weakly dispersed the SPR wavelength λ_R is given by the well-known simplified condition $\epsilon_1(\lambda_R)+2\epsilon_m=0$. As usual, ϵ has been corrected for size reduction by introducing a surface scattering term in its Drude part using[1,35]

$$\epsilon(\lambda)=\epsilon^{\mathrm{bulk}}(\lambda)+\frac{\omega_p^2}{\omega(\omega+i\gamma_{\mathrm{bulk}})}-\frac{\omega_p^2}{\omega(\omega+i\gamma)}, \tag{4}$$

where ϵ^{bulk} is the bulk gold dielectric constant.[36] ω_p is the metal plasma frequency and γ_{bulk} and γ are the electron scattering rates in the bulk and confined metal, respectively, with[1,35]

$$\gamma=\gamma_{\mathrm{bulk}}+2gv_F/D, \tag{5}$$

where v_F is the Fermi velocity and *g* is a proportionality factor on the order of 1.

The measured data are very well reproduced using this approximation, yielding a diameter $D=20.3$ nm, a matrix refractive index $n_m=\sqrt{\epsilon_m}=1.44$, and a surface damping factor $g=1$. Though three parameters are used here they are well defined as, to a large extent, they translate into different spectral features as illustrated in Fig. 6. The overall absolute amplitude of σ_{ext} around and away from the SPR is set by the effective particle diameter *D* (or particle volume *V*) while the surface parameter *g* influences the width of the resonance via modification of ϵ_2 [Eq. (5)]. For gold particles, it mostly shows up in the long wavelength wing of the SPR and in modification of its peak amplitude with respect to the small wavelength interband plateau as shown in Fig. 6(c) for two extreme situations ($g=0.3$ and 2.2). However, for most of the particles investigated here it has a moderate influence on the fitting procedure [inset of Fig. 5(b)], $\epsilon_2(\lambda_R)$ being dominated by its interband contribution in gold.[1,35]

The dielectric constant of the environment ϵ_m is the main parameter setting the spectral shape of σ_{ext}, in particular, the SPR wavelength λ_R. It also influences its peak absolute cross section $\sigma_{\mathrm{ext}}(\lambda_R)$ [Fig. 6(b)] both directly due to the $\epsilon_m^{3/2}$ dependence of σ_{ext} [Eq. (3)] and indirectly due to the change in the SPR width with λ_R (reflecting the dependence of ϵ_2 on λ_R close to the gold interband transition threshold).

The ϵ_m value determined here reflects the surrounding dielectric constant experienced by the nanoparticle. As exten-

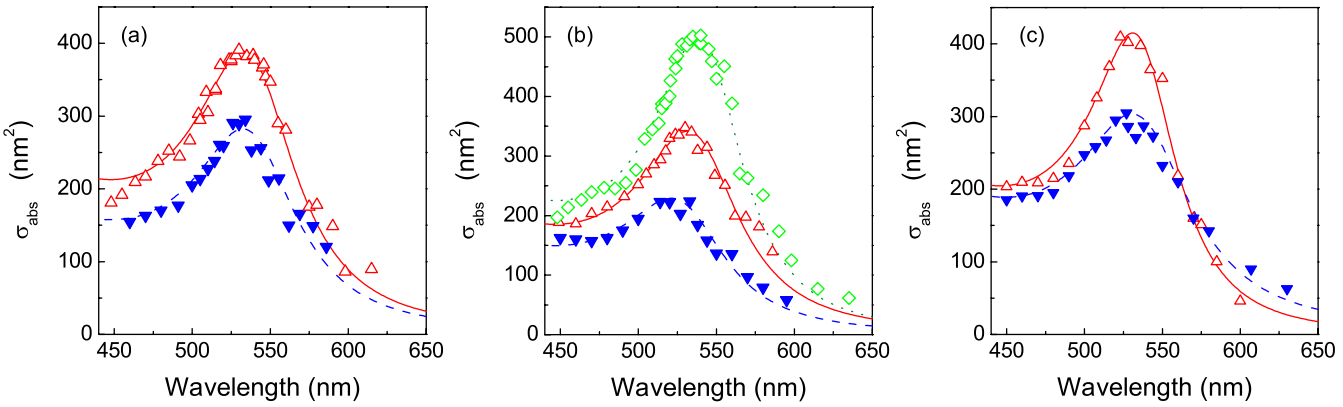

FIG. 6. (Color online) Unpolarized extinction spectra of different single gold nanoparticles whose fits by the spherical quasistatic model [Eq. (3)] only differ by one parameter: (a) Two particles with same environment refractive index $n_m=1.43$ and surface damping factor $g=1.3$, but different diameters $D=18.0$ nm (down-triangles) and $D=19.5$ nm (open up-triangles); (b) three particles with same $D\approx 19$ nm and $g=1.0$, but with $n_m=1.26$ (down-triangles), 1.40 (open up-triangles), and 1.50 (diamonds); (c) two particles with same $D=19.5$ nm and $n_m=1.40$, with $g=2.2$ (down-triangles) and $g=0.3$ (up-triangles).

sively discussed in the sensor context, it corresponds to that of its close environment over a range of the particle size.[28,37–39] The extension over which ϵ_m is probed can be estimated by computing the shell thickness sensitivity of the SPR wavelength of a metal-core/dielectric-shell particle embedded in a dielectric matrix, with dielectric function ϵ, ϵ_s and ϵ_m, respectively.[37] In the quasistatic approximation the absorption cross section of such composite particle takes a similar form as for a sphere, with ϵ_m being replaced in the resonant denominator of Eq. (3) by an effective dielectric function $\epsilon_{\text{eff}}=\epsilon_s(1-a\beta)/(1+2a\beta)$, where a is the core volume fraction: $a=D^3/(D+e)^3$ and $\beta=(\epsilon_s-\epsilon_m)/(\epsilon_s+2\epsilon_m)$.[1,4] Assuming that ϵ_2 is weakly dispersed, the simplified resonance condition $\epsilon+2\epsilon_{\text{eff}}$ can be used and one can readily show that the SPR wavelength dependence on the shell thickness e is given by

$$\frac{\Delta\lambda_R(e)}{\Delta\lambda_R^{\max}}=\frac{1-a}{1+2a(\epsilon_s-\epsilon_m)/(\epsilon_s+2\epsilon_m)}, \tag{6}$$

where $\Delta\lambda_R(e)=\lambda_R(e)-\lambda_R(0)$. $\Delta\lambda_R^{\max}$ is the SPR wavelength modification for a nanosphere when changing its surrounding matrix refractive index from ϵ_m to ϵ_s (i.e., corresponding to the limited value for no and infinitely thick shell, respectively). Note that for usual dielectrics, such as glass or water, the e dependence of the relative SPR shift is actually mostly given by the $1-a$ term in Eq. (6) and is thus almost independent of the nature of the materials. The influence of the matrix thus becomes negligible for a shell thickness on the order of the particle size, the SPR wavelength being then very close to that of a sphere embedded in a ϵ_s matrix (for instance, $\Delta\lambda_R(e)/\Delta\lambda_R^{\max}\geq 0.8$ for $e=D/2$ for gold-core/glass-shell particles in water or vacuum). The SPR wavelength is thus sensitive to a layer on the order of its size around the particle, making it a local probe of its nanoenvironment.[15,28,37–39]

B. Ellipticity effect: Polarized spectra

The impact of the nonsphericity of the particles on the deduced parameters was analyzed performing light polarization dependent measurements. For most investigated particles, the measured σ_{ext} spectra show correlated extrema of the SPR amplitudes and wavelengths for perpendicular polarization directions as illustrated in Fig. 5. This behavior is a signature of a slight nonsphericity of the particle, and as in previous experiments,[14] we have interpreted our data assuming an elliptical nanoparticle shape. As only the particle anisotropy in the x,y plane is detected, one has to make an assumption about its z-direction size. A spheroidal particle of either prolate (p) or oblate (o) shape embedded in a homogeneous environment of dielectric constant ϵ_m has been assumed. The data have then been fitted using[1,4]

$$\sigma_{\text{abs}}^i(\lambda)=\frac{2\pi V\epsilon_m^{3/2}}{\lambda(L_i^{p,o})^2}\frac{\epsilon_2(\lambda)}{|\epsilon(\lambda)+\epsilon_m(1-L_i^{p,o})/L_i^{p,o}|^2}, \tag{7}$$

where light is assumed to be linearly polarized along one of the main axes, i, of the ellipsoid. The geometrical factors $L_i^{p,o}$ only depend on the shape and aspect ratio η of the spheroid defined as the ratio, $\eta=l_s/l_l$, of its short (s) over long (l) axis length.[4] For a close to spherical particle, they can be expanded in $(1-\eta)$ yielding up to second order:

$$L_{l,s}^{p,o}(\eta)=1/3+\alpha_{l,s}^{p,o}(1-\eta), \tag{8}$$

with $\alpha_s^o=-\alpha_l^p=4/15$ and $\alpha_s^p=-\alpha_l^o=2/15$. In polarization-dependent measurements, the aspect ratio thus directly reflects in the displacement of the SPR wavelength for light polarized along the short and long nanoparticle axes. As a first approximation, using the simplified SPR condition,

$$\epsilon_1(\lambda_R^i)+\epsilon_m(1-L_i)/L_i=0, \tag{9}$$

one can show that this displacement is given by

$$\Delta\lambda_{l-s}^{p,o}\approx-\frac{54}{15}(1-\eta)\epsilon_m/\left(\frac{\partial\epsilon_1}{\partial\lambda}\right)_{\lambda_R}, \tag{10}$$

where λ_R is the SPR wavelength for a sphere embedded in the same matrix. For weakly elliptical nanoparticles it is thus independent of the assumed shape, permitting unambiguous extraction of η.

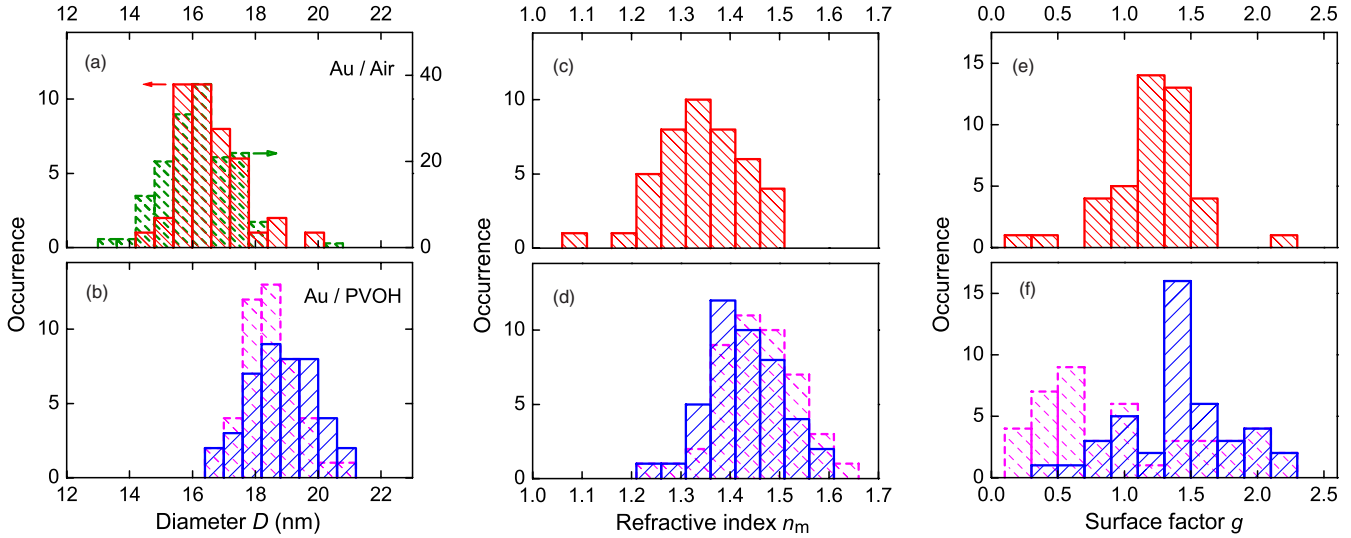

FIG. 7. (Color online) Optically measured distributions of the (a) nanoparticle diameter D (the dashed histogram denotes the results of the TEM measurements), (c) refractive index of the local environment n_m, and (e) electron-surface scattering factor g for gold nanoparticles spin coated on a glass substrate. (b), (d), and (f) show the same data for gold-PVOH solution spin coated onto glass, and spin-coated gold particles postembedded in PVOH (dashed histogram).

In the fitting procedure the surrounding medium dielectric constant ϵ_m is essentially set by the SPR wavelength. Its determination thus also depends on the assumed shape. Using the same approach, switching from a prolate to an oblate shape for the same ϵ_m matrix leads to an identical blue shift of the computed wavelength of the l or s polarized SPR:

$$\Delta\lambda_{l,s}^{p-o} \approx \frac{18}{15}(1-\eta)\epsilon_m \Big/ \left(\frac{\partial\epsilon_1}{\partial\lambda}\right)_{\lambda_R}. \tag{11}$$

When fitting the experimental data, this leads to a reduction in the estimated ϵ_m value of

$$\Delta\epsilon_m^{p_o}/\epsilon_m \approx 3(1-\eta)/5. \tag{12}$$

The shape assumption thus translates in an uncertainty in the extracted n_m value of $\Delta n_m/n_m \approx \pm(3/10)(1-\eta)$, i.e., about 3% for $\eta=0.9$.

Fitting of the polarization-dependent spectra is illustrated Fig. 5(b). The same aspect ratio $\eta=0.91$ has been used assuming a prolate or oblate shape in agreement with the above analysis. Slightly different environment refractive indexes were obtained: $n_m=1.44$ and 1.48, respectively, consistent with the estimated uncertainty. The deduced particle long axis lengths, $2l_l=21.6$ nm and 21 nm, respectively, yield very similar volumes. The estimated equivalent diameters $D_{\mathrm{eq}}^{p,o}$, defined as that of a sphere of same volume, are almost identical ($D_{\mathrm{eq}}^{p}=2\eta^{2/3}l_l=20.3$ nm and $D_{\mathrm{eq}}^{o}=2\eta^{1/3}l_l=20.35$ nm). They are also in excellent agreement with that deduced from the unpolarized spectrum $D=20.3$ nm [Fig. 5(b)]. Note that the measurements with unpolarized light yield a n_m identical to that for the prolate particle assumption. In both cases, prolate or oblate particle, a surface damping factor $g=1$ has been used, identical to that deduced from the unpolarized data [as close to spherical particles were studied, ϵ has been corrected using Eq. (5), replacing D with D_{eq}]. In our gold samples, as long as the particle anisotropy is not investigated, unpolarized light measurement and quasispherical particle approximation are thus sufficient for extracting the particle and environment parameters. Only these will be discussed in the following.

IV. SINGLE NANOPARTICLE: LOCAL CHARACTERIZATION

Using this approach, a random survey of 43 single gold nanoparticles has been investigated in each sample with or without polymer. To avoid any correlation effects, this was done for each sample on five spatially well-separated 20×20 $\mu\mathrm{m}^2$ zones. The distributions of the deduced nanoparticle diameter D, amplitude of the electron-surface scattering correction g, and local environment refractive index n_m are presented in the form of histograms in Fig. 7 (top and bottom graphs in absence and presence of polymer, respectively).

Without polymer, the distribution of the particle size is found to be in excellent agreement with that deduced from TEM measurements [Fig. 7(a)]. Its mean value differs by only about 3%, $\langle D\rangle \approx 16.2$ and 16.6 nm, for TEM and optical measurements, respectively. The data show the same standard deviation of 10% in diameter. Note that the TEM histogram is obtained by averaging the long and short axis projections in the surface plane, while the optical data result from the total volume deduced from Eq. (7). In comparing the results of the two measurements, there is thus an uncertainty of the order $\eta^{1/3}$ in the TEM data, depending on whether the particle under study is a prolate or oblate spheroid.

The same analysis of the optical measurements performed in presence of polymer shows a significant shift of the nanoparticle size histogram [Fig. 7(b)]. Furthermore, analysis of the same sample without polymer and after addition of a polymer drop reveals the same shift, eliminating any possible artifact due to sample deposition or particle selection. The

mean size increases by about 10%, i.e., about 2 nm, to a value of $\langle D\rangle = 18.8$ nm, the standard deviation staying similar. As stressed above, the size of the gold nanoparticle is deduced from its cross-section value. The underlying assumption is that gold is the only absorbing material with an absorption amplitude set by the particle volume and $\epsilon_2(\lambda)$ [Eq. (3)]. Local modification of ϵ_2 or absorption of the surrounding matrix enhanced by the local field effect around the metal nanoparticle can thus translate into a change in the optically estimated particle size. Other absorption enhancement mechanisms can also take place related to charge transfer and surface passivation of the gold nanoparticles by the polymer chains. Though the observed absorption enhancement around the gold surface plasmon resonance is clearly related to the presence of PVOH, definite determination of its origin requires additional measurements.

The deduced refractive index n_m of the local environment shows large particle-to-particle variations [Figs. 7(c) and 7(d)]. Without polymer, it varies from about 1.1 to 1.5, with a mean value $\langle n_m\rangle$ of about 1.34 and a standard deviation of 0.09. It has to be noted that in the above analysis (Sec. III), n_m has been assumed to be homogeneous around the particle, neglecting its asymmetry with the presence of the glass substrate on one side and of air on the other.[5] The estimated n_m thus corresponds to the mean refractive index experienced by the particle. However this simplified approach has been shown to give a correct description of the optical response of deposited nanoparticles using a weighted value of the material refractive index.[21,30,40,41] In our measurements, $\langle n_m\rangle$ lies in between the refractive index of air and glass, but is significantly larger than the square root of their average dielectric function, about 1.27. This increase is consistent with the presence of surfactant molecules bound on the nanoparticle surface and of residual solvent on the sample surface. These variations of the nature of the local environment together with those of the particle-substrate distance are probably at the origin of the fluctuations of the n_m value experienced by the different single nanoparticles.

Similar variations were observed for nanoparticles embedded in the polymer matrix that provide a more homogeneous environment [Fig. 7(d)]. As expected, a larger mean value of $\langle n_m\rangle = 1.44$ is obtained with a slightly smaller standard deviation of about 0.07. The larger $\langle n_m\rangle$ value is consistent with the presence of polymer that increases the surrounding refractive index (the polymer refractive index is in the 1.50–1.53 range). The observed variations are probably due to local changes in the polymer density as well as of the position of the individual particles within the polymer layer, i.e., closer to the polymer-substrate or to the polymer-air interface.[7]

Though the electron-surface scattering factor g has a moderate impact in fitting the measured spectra for the relatively large particles studied here (inset of Fig. 5, except for particles with large g, Fig. 6), its particle-to-particle variation can be estimated. In contrast to the particle diameter and local refractive index, g exhibits very large variations from, typically, 0 to 2.2 [Figs. 7(e) and 7(f)]. These variations have been found to be uncorrelated with those of the local refractive index and were ascribed to the large dependence of the SPR broadening on the close surroundings of the nanoparticle at the interface level.[42] This suggests that the interface conditions largely differ from particle to particle for samples prepared from colloidal solutions. Consequently, the surface contribution to the electron scattering rate can only be properly defined locally at a single-particle level.

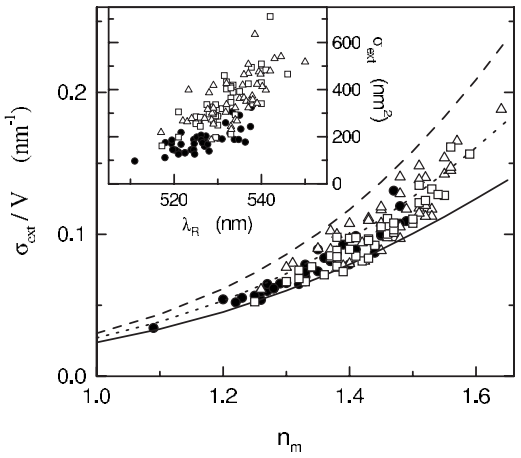

FIG. 8. Experimental peak extinction cross section σ_{ext} divided by the particle volume V as a function of the refractive index of the local environment n_m for all the investigated gold nanoparticles. The different data correspond to nanoparticles spin coated onto a glass substrate without (full dots) or with (open squares) addition of PVOH or postembedded in PVOH after spin coating (open triangles). V and n_m are deduced from fitting the measured individual spectra. The lines show the calculated n_m dependence of σ_{ext} for three values of the electron-surface scattering parameter $g=0$, 1, and 2.2 (dashed, dotted, and full lines, respectively). The inset shows the directly measured σ_{ext} as a function of the SPR wavelength λ_R for the same individual gold nanoparticles. Horizontal and vertical error bars are on the order of the symbol size.

In presence of polymer the mean g values vary from 1.5 to 1 for spin coating the polymer together with the particles or for postembedding them, respectively. An intermediate mean value, $\langle g\rangle = 1.2$, is obtained without polymer (with a narrower distribution). However these variations of $\langle g\rangle$ are probably not connected to the preparation history or nanoparticle embedding environment but rather to the limited number of measurements of a largely varying parameter. The mean g value on the order of 1 suggested by our results is larger than that previously reported in photothermal studies of single gold nanospheres.[43] The origin of this discrepancy is unclear but might be due to different conditions of the nanoparticle surface. In particular, conversely to photothermal measurements for similar sizes,[43] the SPR spectra measured here have always been found to be broader than the computed one using the dielectric constant of bulk gold.

To further stress the impact of the different parameters on the measured amplitude of the extinction cross section, its peak value is plotted as a function of the SPR wavelength in the inset of Fig. 8 for all the investigated nanoparticles. The uncertainties of these measurements are estimated to be about 3 nm in SPR wavelength and 20 nm^2 in cross section, well below the observed variations. For a given SPR wavelength, σ_{ext} shows large fluctuations mostly due to the different volumes of the particle for the same environment. This is

confirmed by the good correlation between the environment refractive index n_m deduced from λ_R and the extinction cross section normalized to the estimated nanoparticle volume (Fig. 8). The observed σ_{ext}/V increase with n_m is consistent with its n_m^3 dependence [Eq. (7)] and to reduction in the width of the SPR (following that of ϵ_2) as it redshifts with increasing n_m (Fig. 8). The measured normalized extinction cross section, σ_{ext}/V, is always smaller than the computed one assuming no surface effects, i.e., $g=0$. It is within the computed value using the quasistatic model for $g=0.2$ and $g=2.2$ (Fig. 8), consistent with the extreme value deduced from fitting the individual spectra. The particle-to-particle variation of g is at the origin of the residual fluctuations of σ_{ext} (Fig. 8).

V. CONCLUSIONS

In conclusion, we have shown that quantitative characterization of a single metal nanoparticle and of its local environment can be performed by comparing the measured extinction cross-section spectra with the spatial modulation technique to theoretical model. For quasispherical gold nanoparticles, the shape assumption made to reproduce the experimental data, i.e., prolate or oblate ellipsoid, does not influence the particle ellipticity estimated from light polarization dependent measurements. It also leads to small uncertainties in the estimated particle properties (volume and surface effects) and dielectric constant of its local environment. In the case of gold, these can be also reliably deduced from polarization averaged spectra interpreted in terms of the spherical quasistatic model. The optically estimated statistic of the nanoparticle size is in excellent agreement with the results of electron microscopy measurements. The surface contribution to the electron scattering rate deduced from the surface plasmon resonance width shows very large particle-to-particle variations, probably due to local surface effect. This suggests that it can only be properly defined locally at the single-particle level. This approach can be extended to the investigation of other absorbing single nano-objects as recently demonstrated for gold nanorods[44] and carbon nanotubes.[45]

The absolute value of the local refractive index of the material surrounding a nanoparticle deduced from these measurements corresponds to its mean value over a shell of about the size of the investigated particle, i.e., on a nanoscale. As compared to scattering-based methods, extinction-based ones thus permit reduction in the probed environment region via reduction in the size of the addressable metal nanoparticle. Furthermore, as the extinction cross section is quantitatively determined, modification of the absorption of a single nanoparticle due to change in its environment can also be detected. This opens up new possibilities for locally investigating the fluctuations of both the refractive and absorptive properties of a matrix at a nanoscale level and for using single metal nanoparticles as quantitative nanoprobes or nanosensors.

ACKNOWLEDGMENTS

M.B. and N.D.F. acknowledge support from Institut Universitaire de France.

*delfatti@lasim.univ-lyon1.fr

[1] U. Kreibig and M. Vollmer, *Optical Properties of Metal Clusters* (Springer, Berlin, 1995).
[2] F. Vallée, N. Del Fatti, and C. Flytzanis, in *Nanostructured Materials*, edited by V. M. Shalaev and M. Moskovits (American Chemical Society, Washington, DC, 1997), p. 70.
[3] F. Vallée, in *Nanomaterials and Nanochemistry*, edited by C. Bréchignac, P. Houdy, and M. Lahmani (Springer, Berlin, 2007), p. 197.
[4] C. F. Bohren and D. R. Huffman, *Absorption and Scattering of Light by Small Particles* (Wiley, New York, 1998).
[5] K. L. Kelly, E. Coronado, L. L. Zhao, and G. C. Schatz, J. Phys. Chem. B **107**, 668 (2003).
[6] Al-Sayed Abdel-Majied Al-Sherbini, Colloids Surf., A **246**, 61 (2004).
[7] T. Itoh, T. Asahi, and H. Masuhara, Jpn. J. Appl. Phys., Part 2 **41**, L76 (2002).
[8] J. J. Mock, D. R. Smith, and S. Schultz, Nano Lett. **3**, 485 (2003).
[9] L. M. Liz-Marzan, Langmuir **22**, 32 (2006).
[10] S. A. Maier, *Plasmonics: Fundamentals and Applications* (Springer, Berlin, 2007).
[11] P. Anger, P. Bharadwaj, and L. Novotny, Phys. Rev. Lett. **96**, 113002 (2006).
[12] S. Kuhn, U. Hakanson, L. Rogobete, and V. Sandoghdar, Phys. Rev. Lett. **97**, 017402 (2006).
[13] M. Danckwerts and L. Novotny, Phys. Rev. Lett. **98**, 026104 (2007).
[14] O. L. Muskens, N. Del Fatti, F. Vallée, J.-R. Huntzinger, P. Billaud, and M. Broyer, Appl. Phys. Lett. **88**, 063109 (2006).
[15] K. Willets and R. Van Duyne, Annu. Rev. Phys. Chem. **58**, 267 (2007), and references therein.
[16] T. Klar, M. Perner, S. Grosse, G. von Plessen, W. Spirkl, and J. Feldmann, Phys. Rev. Lett. **80**, 4249 (1998).
[17] A. A. Mikhailovsky, M. A. Petruska, M. I. Stockman, and V. I. Klimov, Opt. Lett. **28**, 1686 (2003).
[18] A. Liu, A. Rahmani, G. W. Bryant, L. J. Richter, and S. J. Stranick, J. Opt. Soc. Am. A **18**, 704 (2001).
[19] C. Sönnichsen, T. Franzl, T. Wilk, G. von Plessen, and J. Feldmann, New J. Phys. **4**, 93 (2002).
[20] J. J. Mock, M. Barbic, D. R. Smith, D. A. Schultz, and S. Schultz, J. Chem. Phys. **116**, 6755 (2002).
[21] H. Tamaru, H. Kuwata, H. T. Miyazaki, and K. Miyano, Appl. Phys. Lett. **80**, 1826 (2002).
[22] T. Kalkbrenner, U. Hakanson, and V. Sandoghdar, Nano Lett. **4**, 2309 (2004).
[23] K. Lindfors, T. Kalkbrenner, P. Stoller, and V. Sandoghdar, Phys. Rev. Lett. **93**, 037401 (2004).
[24] A. Arbouet, D. Christofilos, N. Del Fatti, F. Vallée, J. R. Huntzinger, L. Arnaud, P. Billaud, and M. Broyer, Phys. Rev. Lett. **93**,

127401 (2004).
[25] S. Berciaud, D. Lasne, G. A. Blab, L. Cognet, and B. Lounis, Phys. Rev. B **73**, 045424 (2006).
[26] G. Raschke, S. Kowarik, T. Franzl, C. Soennischen, T. A. Klar, and J. Feldmann, Nano Lett. **3**, 935 (2003).
[27] L. J. Sherry, R. Jin, C. A. Mirkin, G. C. Schatz, and R. P. Van Duyne, Nano Lett. **6**, 2060 (2006).
[28] A. V. Whitney, J. W. Elam, S. Zou, A. V. Zinonev, P. C. Stair, G. C. Schatz, and R. P. Van Duyne, J. Phys. Chem. B **109**, 20522 (2005).
[29] A. D. McFarland and R. P. Van Duyne, Nano Lett. **3**, 1057 (2003).
[30] P. Billaud, S. Marhaba, E. Cottancin, L. Arnaud, G. Bachelier, C. Bonnet, N. Del Fatti, J. Lermé, F. Vallée, J.-L. Vialle, M. Broyer, and M. Pellarin, J. Phys. Chem. C **112**, 978 (2008).
[31] O. L. Muskens, N. Del Fatti, and F. Vallée, Nano Lett. **6**, 552 (2006).
[32] J. K. Ranka, R. S. Windeler, and A. J. Stentz, Opt. Lett. **25**, 25 (2000).
[33] P. Langot, N. Del Fatti, R. Tommasi, and F. Vallée, Opt. Commun. **137**, 285 (1997).
[34] O. Muskens, D. Christofilos, N. Del Fatti, and F. Vallée, J. Opt. A, Pure Appl. Opt. **8**, S264 (2006).
[35] C. Voisin, N. Del Fatti, D. Christofilos, and F. Vallée, J. Phys. Chem. B **105**, 2264 (2001).
[36] P. B. Johnson and R. W. Christy, Phys. Rev. B **6**, 4370 (1972).
[37] D. D. Evanoff, Jr., R. L. White, and G. Chumanov, J. Phys. Chem. B **108**, 1522 (2004).
[38] M. M. Miller and A. A. Lazarides, *Nanoengineered Assemblies and Advanced Micro-Nanosystems*, MRS Symposia Proceedings No. 820 (Materials Research Society, Pittsburgh, 2004), p. 407.
[39] P. K. Jain and M. A. El-Sayed, Nano Lett. **7**, 2854 (2007).
[40] A. Curry, G. Nusz, A. Chilkoti, and A. Wax, Opt. Express **13**, 2668 (2005).
[41] P. Billaud, J.-R. Huntzinger, E. Cottancin, J. Lermé, M. Pellarin, L. Arnaud, M. Broyer, N. Del Fatti, and F. Vallée, Eur. Phys. J. D **43**, 271 (2007).
[42] H. Hövel, S. Fritz, A. Hilger, U. Kreibig, and M. Vollmer, Phys. Rev. B **48**, 18178 (1993).
[43] S. Berciaud, L. Cognet, P. Tamarat, and B. Lounis, Nano Lett. **5**, 515 (2005).
[44] O. L. Muskens, G. Bachelier, N. Del Fatti, F. Vallée, A. Brioude, X. Jiang, and M. P. Pileni, J. Phys. Chem. C **112**, 8917 (2008).
[45] F. Wang, D. J. Cho, B. Kessler, J. Deslippe, P. J. Schuck, S. G. Louie, A. Zettl, T. F. Heinz, and Y. R. Shen, Phys. Rev. Lett. **99**, 227401 (2007).